Through-Wall Wireless Communication Enabled by a Metalens

Xiangdong Meng,[1] Ruixuan Liu,[2] Hongchen Chu[1,*] Ruwen Peng,[1] Mu Wang,[1]
Yang Hao,[3,†] and Yun Lai[1,‡]

[1] *National Laboratory of Solid State Microstructures, School of Physics, and Collaborative Innovation Center of Advanced Microstructures, Nanjing University, Nanjing 210093, China*

[2] *College of Electronic and Optical Engineering & College of Flexible Electronics (Future Technology), Nanjing University of Posts and Telecommunications, Nanjing 210023, China*

[3] *School of Electronic Engineering and Computer Science, Queen Mary University of London, London, United Kingdom.*

Getting wireless signals around obstacles or passing them through walls is proven to be challenging for electromagnetic waves with a short wavelength and some energy-efficient buildings due to thick insulating materials. Here, we propose a scheme of through-wall wireless communication by applying purposely designed passive metalenses for an asymmetric background medium of the wall. An ultrathin metalens consisting of three layers of metallic patterns is applied to focus the incoming waves to the other side of the wall with high efficiency. The focusing effect is verified by scanning the spatial distribution of electric fields. Due to the focusing effect, the wireless signal strength is significantly enhanced while propagating through the wall. To validate its use in the 5-GHz Wi-Fi environment, we demonstrate that the metalens can reconnect a network channel that is otherwise broken due to weak signal strength, and thus, significantly increase the data transmission rate. Our work opens an unobstructive and retrofitting approach for sustaining wireless communication in future eco-friendly buildings beyond 5G and 6G.

I. INTRODUCTION

Modern wireless-communication technologies, such as Bluetooth [1], Wi-Fi [2], and cellular networks, have greatly changed people's daily life. Recent developments in the 5G cellular network [3] and 5-GHz Wi-Fi offer the benefits of significantly increased bandwidth and connection speed, low latency, and enhanced capacity, but at the cost of reduced areas of coverage (i.e., small cells) due to the shorter wavelengths. Especially, wireless signals at a short wavelength suffer from increased attenuation, when passing through a building's walls; hence, it leads to poor signal reception in indoor environments or adjacent rooms [4–6]. Recent measurement studies performed for frequencies from 800 MHz to 18 GHz revealed the frequency dependence and impact of advanced materials on not only the cellular frequency bands used today (mainly below 3 GHz), but also potential future bands for the 5G and 6G cellular network and beyond. The results show a material-dependent and frequency-dependent attenuation, with an average increase of 20–25 dB in modern constructions of eco-friendly buildings [7]. To overcome this attenuation,

one approach is to further increase the radiation power, but it would consume more electrical power and cause health problems, thus going in the opposite direction of building greener and more sustainable wireless infrastructure [8]. Devices like Wi-Fi extenders are applied to resolve this issue, to a certain extent. However, there is a limit beyond which even the Wi-Fi extender cannot receive any signal. In short, there is huge demand to help wireless signals efficiently penetrate through the wall, such that through-wall wireless communication becomes possible.

Metasurfaces [9–13] may well provide a potentially viable solution to the above challenge. As a layer of subwavelength artificial structures, metasurfaces attract immense attention due to their capabilities to manipulate electromagnetic waves over a broad spectrum from microwaves to optics. Based on metasurfaces, many intriguing phenomena and devices are demonstrated, such as anomalous reflection and refraction [14–16], propagating-to-evanescent wave conversion [17–19], high-efficiency holograms [20–23], ultrathin invisibility cloaks [24–28], the generation of vector optical fields [29,30], metalenses [31–33], and coding metasurfaces [23,34–36]. The application of lensing, i.e., a metalens with ultrathin thickness and flat geometry beyond traditional optical lenses, attracts great interest due to the functionalities of being achromatic and aberration-free

---

*chuhongchen@nju.edu.cn
†y.hao@qmul.ac.uk
‡laiyun@nju.edu.cn

[37–43]. Nevertheless, so far, the majority of metalens studies have focused on applications in a single background, such as free space. Very recently, the concept of a metasurface has been merged with antireflection, and thus, is applied to an asymmetric background [27,28,44,45], i.e., at the interface of two media with a substantial contrast in impedance and refractive index. Some striking phenomena, such as the realization of an "invisible surface" for general dielectrics of arbitrary shape [28] and high-efficiency coupling of microwaves between free space and high-index media [44,45], have been experimentally demonstrated.

Here, we introduce a strategy to utilize a metalens to enhance wireless signals while propagating through a wall, thereby significantly optimizing the signal coverage of wireless communication. With the asymmetric background taken into consideration in the metalens design, the transmittance of wireless signals can be enhanced, and more importantly, the transmitted waves can be focused to a location just behind the wall, where a mobile unit, such as a mobile phone or a Wi-Fi extender, can be installed. Interestingly, the focusing effect can compensate for wave-attenuation loss from building materials within the wall, as verified by both numerical simulations and field-scanning measurements. Finally, we perform a field trial for 5-GHz Wi-Fi communication systems to directly verify the signal boost from the proposed metalens. We clearly observe that an originally disconnected through-wall communication channel can be reconnected by mounting a metalens onto the wall surface. Our approach exhibits distinctive features of polarization independence, broad bandwidth, and unobstructive design. The capability of focusing and redirecting wireless signals for through-wall wireless communications has a significant and wide impact on delivering future eco-friendly and sustainable wireless infrastructure with high-speed and broadband data transmissions.

The concept is schematically shown in Fig. 1. Figure 1(a) shows a typical scenario of wireless signals being attenuated by thick building walls. The reduction of signal strength mainly comes from the following two reasons. The first one is the impedance mismatch between the wall and free space, which leads to reflection. For solid walls composed of bricks and concrete (without considering other factors like rebar), normally, the effective permittivity is around 4–8, and the total reflectance is around 10% to 25%. The second one is the attenuation effect induced by dissipation and inhomogeneity within the wall. In particular, this attenuation increases significantly with frequency for a wall of a fixed thickness. As a result, the signals behind the wall are usually so much weakened that they can no longer be received by mobile phones or Wi-Fi extenders.

Figure 1(b) shows our solution to the above issue based on a passive metalens. When attached to a wall, the metalens is capable of focusing the incoming wave carrying the
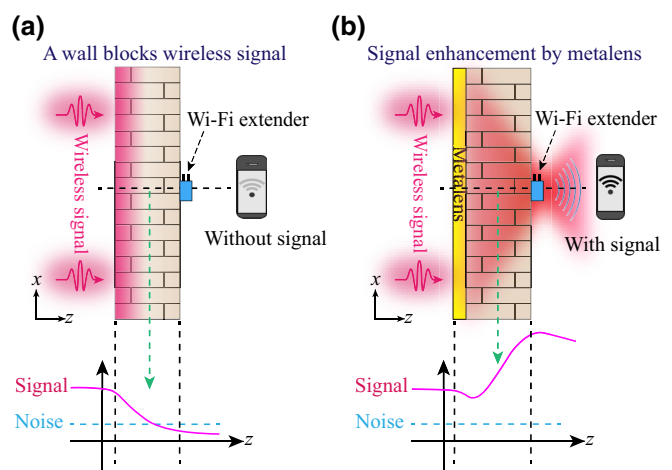

FIG. 1. Illustrative graph of a mechanism to significantly enhance wireless signals penetrating through a wall by a metalens. (a) Wall blocks wireless signals, which could destroy wireless communication. (b) Metalens can help wireless signals transmit through the wall and reestablish wireless communication.

wireless signal to the other side of the wall with high efficiency. Due to the focusing effect, the signal-to-noise ratio is enhanced when the wave penetrates through the wall. Thus, a Wi-Fi extender can receive and pass on the wireless signals at the focal point on the other side of the wall. Such a noninvasive strategy can thus establish a robust and high-speed through-wall communication channel between the two sides of the wall.

II. DESIGN AND NUMERICAL ANALYSIS OF THE METALENS

Here, we demonstrate a case study of 5-GHz Wi-Fi wireless communications, where a through-wall Wi-Fi network at around 5 GHz can be optimized by using the metalens. In the design and simulations, the wall is assumed to have an effective medium of relative permittivity $\varepsilon_w = 5 + 0.11i$, which is reasonable for normal brick walls.

Inspired by previous studies on metasurfaces operating in the asymmetric background [27,28,44,45], here we design the meta-atoms as three-layer metallic structures, as shown in the insets in Figs. 2(a) and 2(b). To achieve the same focusing functionality for microwaves of both polarizations, all the meta-atoms have C_{4v} symmetry. The requirement for the meta-atoms is to cover the range of the $[0, 2\pi)$ transmission phase shift while maintaining a high transmittance from free space into the wall. For ease of design, meta-atoms are composed of three identical layers of metallic patterns (i.e., copper patterns with a thickness of 36 μm), which are separated by two dielectric spacers with relative permittivity $\varepsilon_d = 4.3$ and thickness $h = 3$ mm. The total thickness of the meta-atoms is around 6 mm, i.e., $\lambda/10$, where λ is the wavelength in free space.
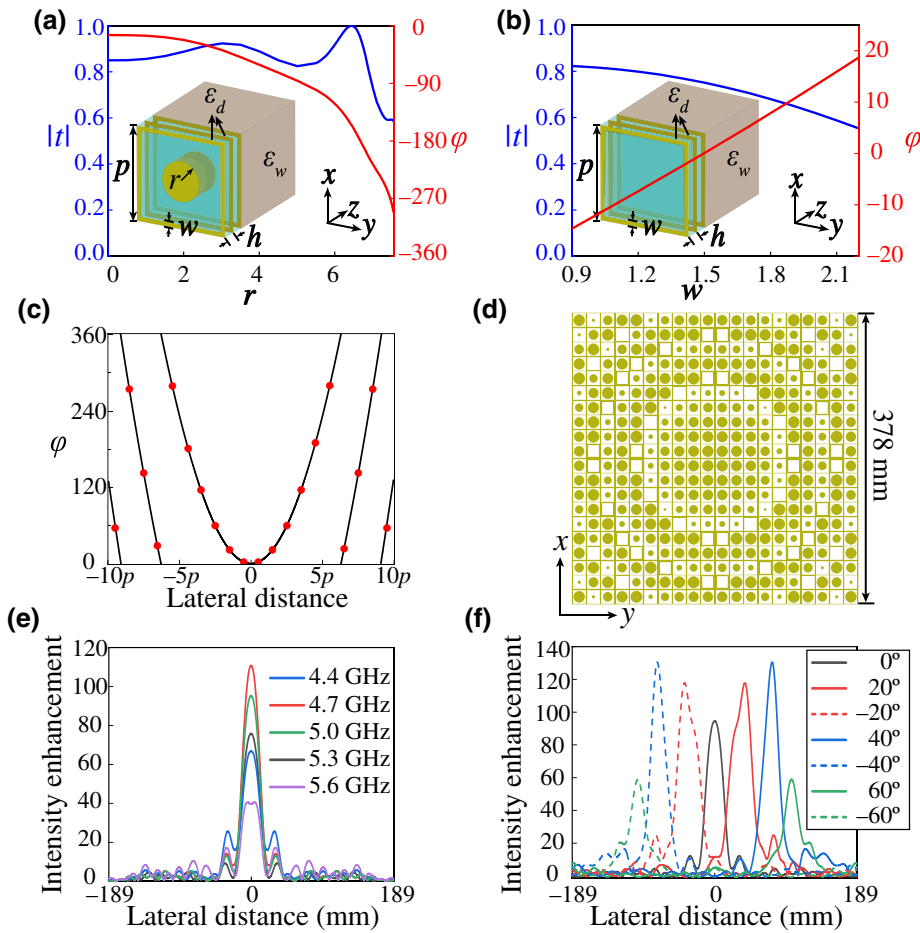
FIG. 2. Design of the metalens operating at an interface between air and a wall. (a) Simulated transmission amplitudes (blue) and transmission phase (red) of the meta-atom as a function of r. (b) Simulated transmission amplitudes (blue) and transmission phase (red) of the meta-atom as a function of w. (c) Phase profile of a metalens with $f = 250$ mm. (d) Schematic view of the designed metalens consisting of 20×20 meta-atoms. Total side length is 378 mm. (e) Simulated field-intensity enhancement of the transmitted wave at 4.4, 4.7, 5.0, 5.3, and 5.6 GHz along the lateral distance across the focal spot in the focal plane. (f) Simulated field-intensity enhancement of the transmitted wave at 5 GHz for different incident angles of $0°$, $\pm20°$, $\pm40°$, and $\pm60°$.

The period of the meta-atoms is set as $p = 18.9$ mm (0.31λ).

Considering an interface between medium 1 and medium 2, and assuming that the incoming waves propagate from medium 1 to medium 2, the transmission coefficient of a meta-atom at the interface is expressed as $t = \sqrt{\left(\cos(\theta_t)\sqrt{\varepsilon_2}\right)/\left(\cos(\theta_i)\sqrt{\varepsilon_1}\right)}E_t/E_i$, so that total transmission corresponds to $|t|^2 = 1$ [28]. Here, E_t and E_i are the complex amplitudes of the electric field of the transmitted and incident waves, respectively; θ_t and θ_i are the transmitted and incident angles, respectively; and ε_1 and ε_2 are the relative permittivities of the media under investigation. The transmission amplitude, $|t|$, and transmission phase, φ, are defined as the amplitude and argument of the transmission coefficients, respectively.

We calculate the transmission coefficient of the meta-atoms in the asymmetric background by using CST Microwave Studio simulation software. Unit-cell boundary conditions are applied in the x and y directions, while the wave ports are applied in the z direction. The port mode with minimum order is selected to excite an incident plane wave. In Figs. 2(a) and 2(b), we demonstrate the calculated transmission amplitude, $|t|$, and transmission phase, φ, at 5 GHz for two types of meta-atoms with different

patterns. The first pattern is composed of a square metallic strip with a fixed width of $w = 0.9$ mm and a metallic circle with varying radius, r, from 0 to 7.61 mm. The second pattern is only a square metallic strip with varying width, w, from 0.9 to 2.2 mm. Due to the limit of unit-cell boundaries, the loss of the background is ignored here but considered in the rest of this work. From Figs. 2(a) and 2(b), it is observed that the meta-atoms can achieve a relatively high transmission amplitude (on average, above 0.85) that allows the incoming waves to transmit into the wall at high efficiency. Moreover, the combined transmission phase shifts of the two types of meta-atoms can almost cover the range of $[0, 2\pi)$, as required in the metasurface design.

According to Fermat's principle, the transmission phase distribution of the metalens operating at an interface between free space and a medium of relative permittivity ε_w can be expressed as

$$\varphi(R) = -\frac{2\pi\sqrt{\varepsilon_w}}{\lambda}\left(\sqrt{f^2 + R^2} - f\right) + \varphi_0, \qquad (1)$$

where φ_0 is a constant phase shift, f is the desired focal length, and R is the distance between the position on the metalens and the center of the metalens. In this

case, we assume a focal length of 250 mm, i.e., $f = 250$ mm. Figure 2(c) shows the transmission phase distribution along the x direction. The red points marked in Fig. 2(c) represent the discretized transmission phase of the meta-atoms designed according to Figs. 2(a) and 2(b). Figure 2(d) shows the designed metalens consisting of 20×20 meta-atoms. The side length of the metalens is 378 mm. The detailed geometric parameters of these meta-atoms are listed in Sec. 1 within the Supplemental Material [46]. We then simulate the field-intensity profiles of the designed metalens attached to a wall with $\varepsilon_w = 5 + 0.11i$ and a thickness of 220 mm under normal incidence. Figure 2(e) shows the simulated field-intensity enhancement along the lateral distance across the focal point in the focal plane at different frequencies. Obviously, the metalens has a distinct focusing functionality in the frequency range from 4.4 to 5.6 GHz, which implies that the metalens function has a bandwidth of around 1.2 GHz. Specifically, the enhancement is 95.3 times at the focal point at 5 GHz. At 4.7 GHz, such enhancement is up to 110.8 times. We note that this metalens is insensitive to polarization due to the C_{4v} symmetry of each meta-atom and the whole metalens.

We also investigate the performance of the designed metalens under oblique incident waves. The simulated results show that the focusing effect of the metalens is remarkable within $\pm 60°$, as shown in Fig. 2(f). In addition, the metalens can be further redesigned by changing the distribution pattern of the meta-atoms, according to the wave front of incidence in real-world applications. Without loss of generality, here, we consider only the case of normal incidence as a proof of principle. But, as pointed out earlier, the same meta-atom design can be used for more practical scenarios.

III. EXPERIMENTAL DEMONSTRATION OF SIGNAL ENHANCEMENT

First, we experimentally verify the focusing effect of the metalens. The designed metalens is fabricated by using the mature circuit-board-etching technology, as shown in Fig. 3(a). The experimental setup is shown in Fig. 3(b). A brick wall 220 mm thick (slightly shorter than the focal distance, f), 1200 mm wide, and 848 mm high is constructed to block the wireless signals. The relative permittivity of the brick is measured to be $4.7 + 0.11i$, which is close to the assumption in the metalens design, i.e., $\varepsilon_w = 5 + 0.11i$. Due to the limited size of the brick wall, foam absorbers are placed near the wall to minimize waves bypassing the brick wall instead of penetrating it. The reflectance, transmittance, and absorptance of the brick wall are measured by using horn antennas, as shown in Sec. 2 within the Supplemental Material [46]. Around the working frequency of 5 GHz, the transmittance of the wall is quite low, i.e.,
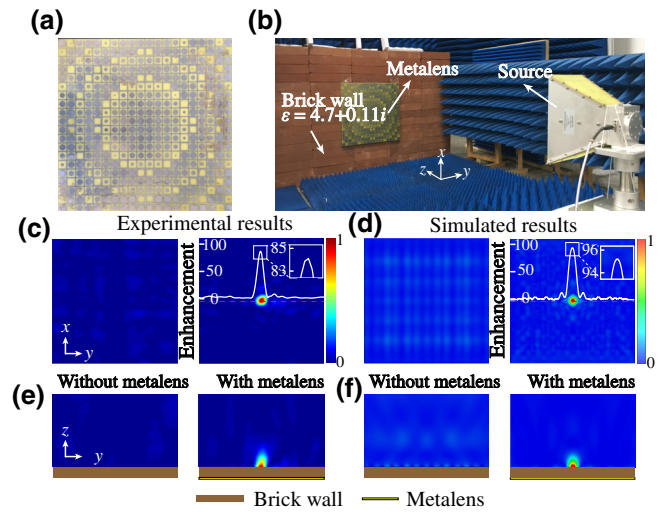

FIG. 3. Experimental demonstration of wave focusing and signal enhancement by the metalens. (a) Photograph of the fabricated metalens. (b) Experimental setup and measurement environment for characterizing the metalens. Measured field-intensity distributions along the (c) x-y plane and (e) y-z plane under normal incidence at 5 GHz for cases with and without the metalens. Inset in (c) shows the measured field-intensity enhancement of the transmitted wave along the red dashed line. Simulated field-intensity distributions along the (d) x-y plane and (f) y-z plane under normal incidence at 5 GHz for cases with and without the metalens. Inset in (d) shows the simulated field-intensity enhancement of the transmitted wave along the red dashed line.

about 20%. With such a low transmittance, this wall can significantly attenuate the signal strength of 5-GHz Wi-Fi.

Then, the metalens is attached to the brick wall, as shown in Fig. 3(b). Such a metalens can focus the incoming waves at the focal point, which is located just behind the brick wall. To verify the focusing effect, a receiving antenna is placed on a moving stage to measure the near field behind the brick wall. The emitting horn antenna and receiving antenna are connected to the Vector Network Analyzer (KEYSIGHT N5224B) to acquire the magnitude and phase of the transmitted waves. The measured field-intensity distributions of the electric fields behind the wall are plotted in Fig. 3(c) (x-y plane) and 3(e) (y-z plane), respectively, for the two cases with and without the metalens at 5 GHz. From Figs. 3(c) and 3(e), we observe a distinct focal spot of high field intensity just behind the wall, when the metalens is attached to the front surface of the wall. On the contrary, when the metalens is absent, the field intensity behind the wall is much smaller throughout the whole region. The measured field-intensity enhancement of the transmitted wave by the metalens at the focal point in the x-y plane is 84.4 times. For comparison, we also calculate the field-intensity profiles behind the wall by numerical simulations. The simulated field-intensity distributions of the electric fields in the x-y and y-z planes for

the two cases with and without the metalens are, respectively, shown in Figs. 3(d) and 3(f), and it is found that the field-intensity enhancement at the focal point is up to 95.3 times. Clearly, the measured results are in excellent agreement with the simulation results; this confirms that the designed metalens can efficiently focus the incoming wave through the brick wall at 5 GHz. The small discrepancy in the field-intensity enhancements in the experiment can be attributed to other factors like the inhomogeneity of the brick wall, the small air gap between the metalens and the brick wall, and the small fabrication error of the metalens.

In addition, we also use a homogenous dielectric wall to verify the function of the metalens. The measurement results are consistent with those of the real brick wall (more details are provided in Sec. 3 within the Supplemental Material [46]).

Next, we carry out two types of wireless-communication experiments, which are referred to as schemes 1 and 2, respectively. The experimental setup for scheme 1 is shown in Fig. 4(a). A commercial 5-GHz Wi-Fi router with a transmitted power of 25 mW is set at the 36th channel, with a center frequency of 5.18 GHz and a bandwidth of 40 MHz. The 5-GHz Wi-Fi router is 2 m away

from the wall and placed inside a box made of foam absorbers and aluminum foil to mimic the 5-GHz Wi-Fi source with low-energy radiation. The transmitted power can be controlled by adjusting the number of layers of foam absorbers, and we manage to realize three levels of transmitted power, which are denoted as I, II, and III. For transmitted power I, the average signal strength in front of the wall is measured to be −67.3 dBm. However, when a mobile phone is placed on the other side of the wall, it cannot detect the wireless signal (below the minimum limit of −80 dBm), and therefore, the network is disconnected, as shown in Fig. 4(b). The download and upload speeds are thus reduced to zero.

Remarkably, when the metalens is attached to the front surface of the brick wall, the 5-GHz Wi-Fi network is reconnected, and the download and upload speeds are measured to be 83.3 and 88.6 Mbps, respectively, as shown in Fig. 4(c). Ten repeated measurements are carried out for scheme 1, with and without the metalens, under three levels of transmitted power. The average values of the measured download and upload speeds, signal strength, and packet latency with standard errors are plotted in Fig. 4(d). Under transmitted power I, the average signal strength behind the wall is −48 dBm, which indicates an
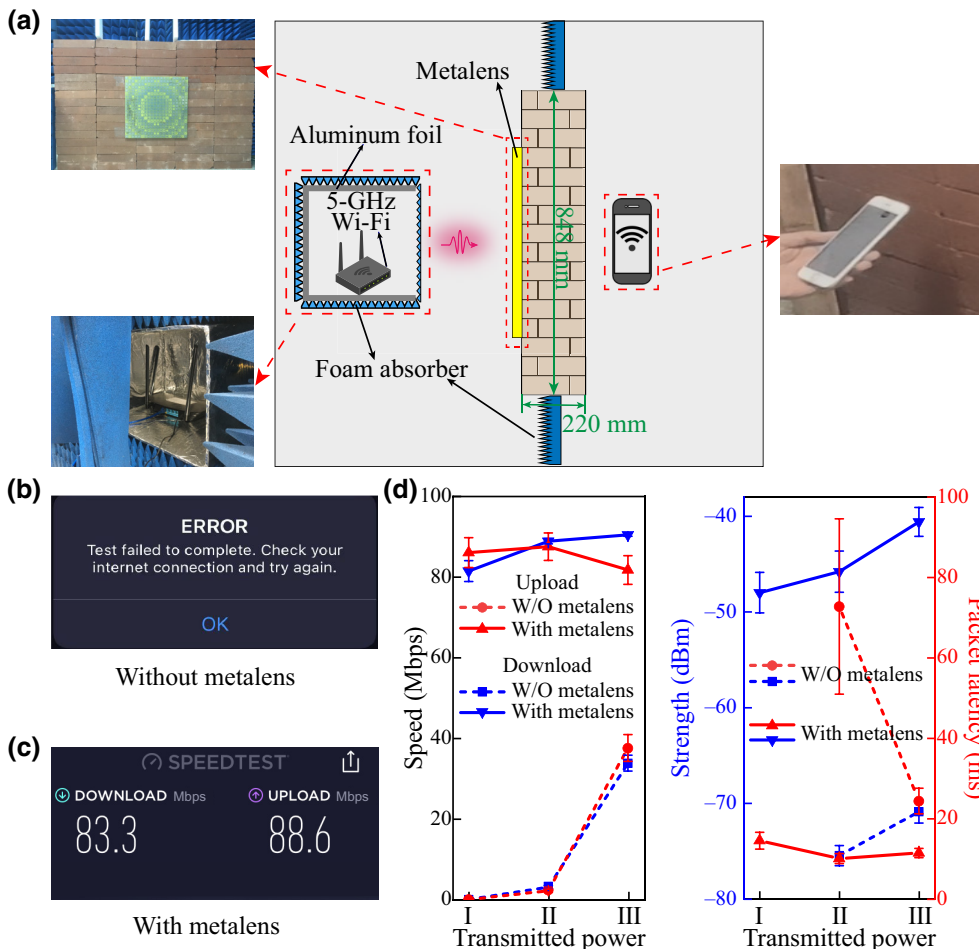

FIG. 4. Experimental demonstration of through-wall wireless communication for 5-GHz Wi-Fi network based on the metalens (scheme 1). (a) Experimental setup in scheme 1. 5-GHz Wi-Fi router is surrounded by wave-absorbing materials and placed 2 m away from the wall, and a mobile phone is placed near the focal point of the metalens. (b) Speed-test result without a metalens under transmitted power I: failed network connection. (c) Speed-test result with a metalens under transmitted power I: network speeds measured to be 83.3 Mbps (download) and 88.6 Mbps (upload). (d) Average download and upload speeds, signal strength, and packet latency for repeated measurements with and without the metalens, under three levels of transmitted power. Error bars represent standard errors of measurement results.

over 30 dB enhancement over the case without a metal-ens. The average download and upload speeds in repeated measurements are 81.77 and 86.39 Mbps, respectively. The packet latency is 14.437 ms. We note that the speeds are close to the measured maximum speeds of our equipment and network (download speed of 93.64 Mbps and upload speed of 93.20 Mbps).

Then we slightly increase the transmitted power to level II, where the average signal strength in front of the wall is increased to -66.9 dBm. We find that the network is connected even when the metalens is absent, but the average download and upload speeds are quite low, i.e., 3.09 and 2.17 Mbps, respectively. When the metalens is attached to the wall, the quality of the wireless network is significantly improved, as shown in Fig. 4(d). The average

download and upload speeds are 89.19 and 87.85 Mbps, respectively, and the signal strength and the packet latency are -45.8 dBm and 9.967 ms, respectively; these values indicate that the network is much better than that without the metalens. We further increase the transmitted power to level III, where the average signal strength in front of the wall is increased to -58.8 dBm. From the results, we find that the metalens can still lead to significant improvements in the download and upload speeds, strength, and packet latency. More details of this experiment are shown in Video S1 within the Supplemental Material, and raw data of the measurements are shown in Sec. 4 within the Supplemental Material [46].

Next, we consider scheme 2, in which a Wi-Fi extender is placed at the focal point of the metalens, and the
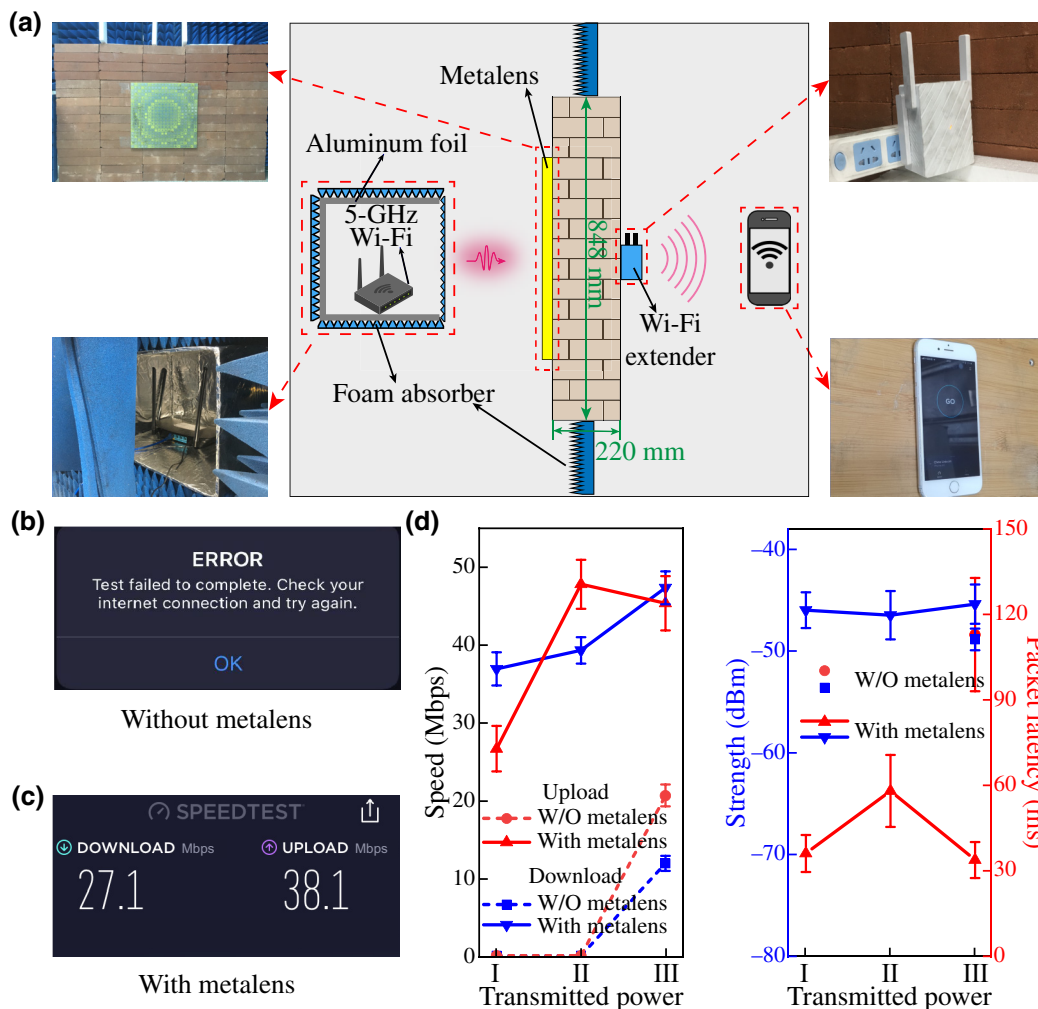

FIG. 5.   Experimental demonstration of through-wall wireless communication for 5-GHz Wi-Fi network based on the metalens and Wi-Fi extender (scheme 2). (a) Experimental setup in scheme 2. Wi-Fi extender is placed at the focal point of the metalens, and the mobile phone is positioned away from the focal point. (b) Speed-test result without a metalens under transmitted power I: failed network connection. (c) Speed-test result with a metalens under transmitted power I: network speeds measured to be 27.1 Mbps (download) and 38.1 Mbps (upload). (d) Average download and upload speeds, signal strength, and packet latency for repeated measurements with and without the metalens, under three levels of transmitted power. Error bars represent standard errors of measurement results.

mobile phone can be connected to the Wi-Fi extender over a considerable distance, as shown in Fig. 5(a). The Wi-Fi extender functions as a bridge linking the 5-GHz Wi-Fi router and the mobile phone. In this case, we also manage to realize three levels of transmitted power (denoted as I, II, and III) by adjusting the number of layers of the foam absorbers as well as the position of the Wi-Fi router. Under transmitted powers I and II, when the metalens is absent, the Wi-Fi extender cannot connect to the 5-GHz Wi-Fi router, thus the network channel is down, as shown in Fig. 5(b). On the contrary, when the metalens is attached to the front surface of the brick wall, the wireless network is reconnected. Under transmitted power I, the download and upload speeds are measured to be 27.1 and 38.1 Mbps, respectively, as shown in Fig. 5(c). We further perform repeated measurements with and without the metalens, under the three levels of transmitted power. The average results are plotted with standard errors in Fig. 5(d). Clearly, for all three levels of transmitted power, the metalens can reconnect or improve the wireless network. We note that the measured speeds are lower than those in Fig. 4; this is due to the effect of the Wi-Fi extender. The progress of the experiment is recorded and shown in Video S2 within the Supplemental Material, and raw data of repeated measurements are shown in Sec. 5 within the Supplemental Material [46]. Both experiments of schemes 1 and 2 show that the designed metalens enables through-wall wireless communication, which is crucial for future high-frequency wireless communication.

IV. DISCUSSION AND CONCLUSION

Previously, active metasurfaces, also denoted as smart surfaces [47–50], were demonstrated to effectively optimize the signal strength in wireless communication. Such smart surfaces, made of tunable electronic components, aim to flexibly control beam forming and focusing in free space. Some other schemes based on reflective metasurfaces are also applied to enhance signal strength [51,52]. Nevertheless, most previous research focused on routing wireless signals to bypass the obstacles in free space. The possibility of allowing wireless signals to penetrate through walls with high efficiency has not been demonstrated. Here, through designing a passive metalens for asymmetric backgrounds, we clearly prove the validity of through-wall wireless communication via metalenses. With the help of a Wi-Fi extender, the signal penetrating through the wall can be passed on to all mobile devices behind the wall, thereby establishing a through-wall network channel. This strategy is less complicated, passive, and cost-effective.

To achieve high efficiency, such a transmissive metalens requires not only the correct phase modulation but also high transmittance through the surface of walls. Such a capability to achieve impedance matching within a deep

subwavelength scale was recently realized by metamaterials [53], multilayer or cascaded metasurfaces [28,44], bianisotropic metamaterials [45], etc. The coalescence of antireflection and wave-front control opens a pathway towards interface optics with high efficiency. Here, we adopt a relatively simple meta-atom design of three identical metallic patterns, because the effects of focusing and signal enhancement are already prominent, as shown in the proof-of-principle experiments. In the future, the metallic patterns of the meta-atoms can be further optimized for more challenging situations, such as thicker walls, larger impedance mismatch, and absorption.

In conclusion, we hereby report a noninvasive method to enable or enhance through-wall wireless communication. We show that an ultrathin passive metalens can help wireless signals penetrate through obstacles, such as walls. The focusing effect can effectively compensate for loss within the wall, thus maintaining a large signal-to-noise ratio on the other side of the wall. Such a focusing effect, as well as the reconnection of a 5-GHz Wi-Fi network channel through the wall by applying the metalens, is experimentally demonstrated. Our work proposes and demonstrates a practical route to solve the critical issue of signal attenuation through walls, which could benefit next-generation wireless systems based on higher frequencies.

[1] J. C. Haartsen, The Bluetooth radio system, IEEE Pers. Commun. **7**, 28 (2000).

[2] D. Niyato and E. Hossain, Wireless broadband access: Wimax and beyond - integration of WiMAX and WiFi: Optimal pricing for bandwidth sharing, IEEE Commun. Mag. **45**, 140 (2007).

[3] G. L. Stüber, *Principles of mobile communication*, 4th ed. (Springer, Cham, 2017).

[4] G. Yang, J. Du, and M. Xiao, Maximum throughput path selection with random blockage for indoor 60 GHz relay networks, IEEE Trans. Commun. **63**, 3511 (2015).

[5] S. Mumtaz, J. Rodriguez, and L. Dai, *MmWave massive MIMO: A paradigm for 5G* (Academic Press, London, 2016).

[6] S. A. Busari, S. Mumtaz, S. Al-Rubaye, and J. Rodriguez, 5G millimeter-wave mobile broadband: Performance and challenges, IEEE Commun. Mag. **56**, 137 (2018).

[7] E. Greenberg and G. Segal, in *2020 14th European Conference on Antennas and Propagation (EuCAP)* (IEEE, Copenhagen, Denmark, 2020), p. 1.

[8] L. Shao, R. Foster, M. Coleman, K. Irvine, M. Lemon, and Y. Hao, Wireless energy behaviour monitoring (Wi-be) for office buildings, Int. J. Low Carbon Technol. **12**, 181 (2017).

[9] A. V. Kildishev, A. Boltasseva, and V. M. Shalaev, Planar photonics with metasurfaces, Science **339**, 1232009 (2013).

[10] N. Yu and F. Capasso, Flat optics with designer metasurfaces, Nat. Mater. **13**, 139 (2014).

[11] Y. Xu, Y. Fu, and H. Chen, Planar gradient metamaterials, Nat. Rev. Mater. **1**, 16067 (2016).

[12] Q. He, S. Sun, S. Xiao, and L. Zhou, High-efficiency metasurfaces: Principles, realizations, and applications, Adv. Opt. Mater. **6**, 1800415 (2018).

[13] S. Sun, Q. He, J. Hao, S. Xiao, and L. Zhou, Electromagnetic metasurfaces: Physics and applications, Adv. Opt. Photonics **11**, 380 (2019).

[14] N. Yu, P. Genevet, M. A. Kats, F. Aieta, J.-P. Tetienne, F. Capasso, and Z. Gaburro, Light propagation with phase discontinuities: Generalized laws of reflection and refraction, Science **334**, 333 (2011).

[15] F. Aieta, P. Genevet, N. Yu, M. A. Kats, Z. Gaburro, and F. Capasso, Out-of-plane reflection and refraction of light by anisotropic optical antenna metasurfaces with phase discontinuities, Nano Lett. **12**, 1702 (2012).

[16] X. Ni, N. K. Emani, A. V. Kildishev, A. Boltasseva, and V. M. Shalaev, Broadband light bending with plasmonic nanoantennas, Science **335**, 427 (2012).

[17] S. Sun, Q. He, S. Xiao, Q. Xu, X. Li, and L. Zhou, Gradient-index meta-surfaces as a bridge linking propagating waves and surface waves, Nat. Mater. **11**, 426 (2012).

[18] H. Chu, J. Luo, and Y. Lai, Efficient way to convert propagating waves into guided waves via gradient wire structures, Opt. Lett. **41**, 3551 (2016).

[19] W. Sun, Q. He, S. Sun, and L. Zhou, High-efficiency surface plasmon meta-couplers: Concept and microwave-regime realizations, Light Sci. Appl. **5**, e16003 (2016).

[20] G. Zheng, H. Mühlenbernd, M. Kenney, G. Li, T. Zentgraf, and S. Zhang, Metasurface holograms reaching 80% efficiency, Nat. Nanotechnol. **10**, 308 (2015).

[21] L. Huang, S. Zhang, and T. Zentgraf, Metasurface holography: From fundamentals to applications, Nanophotonics **7**, 1169 (2018).

[22] Z.-L. Deng, M. Jin, X. Ye, S. Wang, T. Shi, J. Deng, N. Mao, Y. Cao, B.-O. Guan, A. Alù, *et al.*, Full-color complex-amplitude vectorial holograms based on multi-freedom metasurfaces, Adv. Funct. Mater. **30**, 1910610 (2020).

[23] L. Li, T. J. Cui, W. Ji, S. Liu, J. Ding, X. Wan, Y. B. Li, M. Jiang, C.-W. Qiu, and S. Zhang, Electromagnetic reprogrammable coding-metasurface holograms, Nat. Commun. **8**, 197 (2017).

[24] J. Zhang, Z. Mei, W. Zhang, F. Yang, and T. J. Cui, An ultrathin directional carpet cloak based on generalized Snell's law, Appl. Phys. Lett. **103**, 151115 (2013).

[25] X. Ni, Z. J. Wong, M. Mrejen, Y. Wang, and X. Zhang, An ultrathin invisibility skin cloak for visible light, Science **349**, 1310 (2015).

[26] B. Orazbayev, N. M. Estakhri, M. Beruete, and A. Alù, Terahertz carpet cloak based on a ring resonator metasurface, Phys. Rev. B **91**, 195444 (2015).

[27] H. Chu, Q. Li, B. Liu, J. Luo, S. Sun, Z. Hang, L. Zhou, and Y. Lai, A hybrid invisibility cloak based on integration of transparent metasurfaces and zero-index materials, Light Sci. Appl. **7**, 50 (2018).

[28] H. Chu, H. Zhang, Y. Zhang, R. Peng, M. Wang, Y. Hao, and Y. Lai, Invisible surfaces enabled by the coalescence of anti-reflection and wavefront controllability in ultrathin metasurfaces, Nat. Commun. **12**, 4523 (2021).

[29] E. Karimi, S. A. Schulz, I. D. Leon, H. Qassim, J. Upham, and R. W. Boyd, Generating optical orbital angular momentum at visible wavelengths using a plasmonic metasurface, Light Sci. Appl. **3**, e167 (2014).

[30] A. Forbes, M. de Oliveira, and M. R. Dennis, Structured light, Nat. Photonics **15**, 253 (2021).

[31] C. Ma and Z. Liu, A super resolution metalens with phase compensation mechanism, Appl. Phys. Lett. **96**, 183103 (2010).

[32] M. Khorasaninejad, W. T. Chen, R. C. Devlin, J. Oh, A. Y. Zhu, and F. Capasso, Metalenses at visible wavelengths: Diffraction-limited focusing and subwavelength resolution imaging, Science **352**, 1190 (2016).

[33] M. Khorasaninejad and F. Capasso, Metalenses: Versatile multifunctional photonic components, Science **358**, eaam8100 (2017).

[34] T. J. Cui, M. Q. Qi, X. Wan, J. Zhao, and Q. Cheng, Coding metamaterials, digital metamaterials and programmable metamaterials, Light Sci. Appl. **3**, e218 (2014).

[35] L.-H. Gao, Q. Cheng, J. Yang, S.-J. Ma, J. Zhao, S. Liu, H.-B. Chen, Q. He, W.-X. Jiang, H.-F. Ma, *et al.*, Broadband diffusion of terahertz waves by multi-bit coding metasurfaces, Light Sci. Appl. **4**, e324 (2015).

[36] L. Zhang, X. Q. Chen, S. Liu, Q. Zhang, J. Zhao, J. Y. Dai, G. D. Bai, X. Wan, Q. Cheng, G. Castaldi, *et al.*, Space-time-coding digital metasurfaces, Nat. Commun. **9**, 4334 (2018).

[37] F. Aieta, M. A. Kats, P. Genevet, and F. Capasso, Multi-wavelength achromatic metasurfaces by dispersive phase compensation, Science **347**, 1342 (2015).

[38] A. Arbabi, E. Arbabi, S. M. Kamali, Y. Horie, S. Han, and A. Faraon, Miniature optical planar camera based on a wide-angle metasurface doublet corrected for monochromatic aberrations, Nat. Commun. **7**, 13682 (2016).

[39] S. Wang, P. C. Wu, V.-C. Su, Y.-C. Lai, C. H. Chu, J.-W. Chen, S.-H. Lu, J. Chen, B. Xu, C.-H. Kuan, *et al.*, Broadband achromatic optical metasurface devices, Nat. Commun. **8**, 187 (2017).

[40] W. T. Chen, A. Y. Zhu, V. Sanjeev, M. Khorasaninejad, Z. Shi, E. Lee, and F. Capasso, A broadband achromatic metalens for focusing and imaging in the visible, Nat. Nanotechnol. **13**, 220 (2018).

[41] S. Shrestha, A. C. Overvig, M. Lu, A. Stein, and N. Yu, Broadband achromatic dielectric metalenses, Light Sci. Appl. **7**, 85 (2018).

[42] S. Wang, P. C. Wu, V.-C. Su, Y.-C. Lai, M.-K. Chen, H. Y. Kuo, B. H. Chen, Y. H. Chen, T.-T. Huang, J.-H. Wang,

et al., A broadband achromatic metalens in the visible, Nat. Nanotechnol. **13,** 227 (2018).

[43] R. J. Lin, V.-C. Su, S. Wang, M. K. Chen, T. L. Chung, Y. H. Chen, H. Y. Kuo, J.-W. Chen, J. Chen, Y.-T. Huang, *et al.*, Achromatic metalens array for full-colour light-field imaging, Nat. Nanotechnol. **14,** 227 (2019).

[44] F. Yang, B. O. Raeker, D. T. Nguyen, J. D. Miller, Z. Xiong, A. Grbic, and J. S. Ho, Antireflection and Wavefront Manipulation with Cascaded Metasurfaces, Phys. Rev. Appl. **14,** 064044 (2020).

[45] G. Lavigne and C. Caloz, Generalized Brewster effect using bianisotropic metasurfaces, Opt. Express **29,** 11361 (2021).

[46] See the Supplemental Material at http://link.aps.org/supple mental/10.1103/PhysRevApplied.17.064027 for the details of the meta-atoms; the measured reflectance, transmittance, and absorbance of the brick wall; an experimental demonstration of wave focusing through a homogenous dielectric wall; raw data supporting plots in Figs. 4 and 5; and videos that record details of the measurements.

[47] V. Arun and H. Balakrishnan, in *17th USENIX Symposium on Networked Systems Design and Implementation (NSDI 20)* (USENIX Association, Santa Clara, CA, 2020), p. 1047.

[48] H. Zhao, Y. Shuang, M. Wei, T. J. Cui, P. d. Hougne, and L. Li, Metasurface-assisted massive backscatter wireless communication with commodity Wi-Fi signals, Nat. Commun. **11,** 3926 (2020).

[49] L. Zhang, M. Z. Chen, W. Tang, J. Y. Dai, L. Miao, X. Y. Zhou, S. Jin, Q. Cheng, and T. J. Cui, A wireless communication scheme based on space- and frequency-division multiplexing using digital metasurfaces, Nat. Electron. **4,** 218 (2021).

[50] X. Pei, H. Yin, L. Tan, L. Cao, Z. Li, K. Wang, K. Zhang, and E. Björnson, RIS-aided wireless communications: Prototyping, adaptive beamforming, and indoor/outdoor field trials, IEEE Trans. Commun. **69,** 8627 (2021).

[51] S. V. Hum and J. Perruisseau-Carrier, Reconfigurable reflectarrays and array lenses for dynamic antenna beam control: A review, IEEE Trans. Antennas Propag. **62,** 183 (2014).

[52] Q. Wu and R. Zhang, Intelligent reflecting surface enhanced wireless network via joint active and passive beamforming, IEEE Trans. Wirel. Commun. **18,** 5394 (2019).

[53] H. T. Chen, J. Zhou' J. F. O'Hara, F. Chen, A. K. Azad, and A. J. Taylor, Antireflection Coating Using Metamaterials and Identification of Its Mechanism, Phys. Rev. Lett. **105,** 073901 (2010).